Microchimica Acta (2021) 188: 328
https://doi.org/10.1007/s00604-021-04999-4

ORIGINAL PAPER

An enhanced photoelectrochemical biosensor for colitoxin DNA based on HKUST-1/TiO_2 and derived HKUST-CuO/TiO_2 heterogeneous composites

Delun Zheng[1,2] · Min Chen[3] · Jingjun Peng[1] · Jiayang Chen[1] · Tufeng Chen[1] · Yaowen Chen[1] · Linjia Huang[4] · Wenhua Gao[1]

Received: 12 May 2021 / Accepted: 24 August 2021 / Published online: 8 September 2021

Abstract

HKUST-1 MOFs and its derivative HKUST-CuO were coupled with TiO_2 nanoparticles to form the heterogeneous composites of HKUST-1/TiO_2 and HKUST-CuO/TiO_2 based on their well-suitable bandgap energies (Eg). Compared with mono-component HKUST-1 or HKUST-CuO, the prepared composites displayed photoelectrochemical (PEC) response due to the synergistic effect from their heterogeneous structure. Higher photocurrent response was obtained on HKUST-CuO/TiO_2-modified ITO electrode (HKUST-CuO/TiO_2/ITO), which could be attributed to the hollow structure with a thin shell of HKUST-CuO greatly enhancing visible spectra harvesting. The CuO component in HKUST-CuO not only could accelerate electron transfer on the heterojunction interface but also effectively separate the photo-generated charge carriers (e^{-1}/h^{+}). Based on the excellent PEC performance of prepared photoactive composite material, under visible-light excitation ($\lambda \geq 420$ nm) and with a working potential of 0 V (vs. Ag/AgCl), the S1 (probe DNA)/HKUST-CuO/TiO_2/ITO PEC platform was successfully fabricated for colitoxin DNA detection without using ascorbic acid (AA) as an electron donor. Compared with the analysis results on S1/HKUST-1/TiO_2/ITO electrode, S1/HKUST-CuO/TiO_2/ITO displayed a wider linear response range from 1.0×10^{-6} to 4.0×10^{-1} nM with a lower detection limit of 3.73×10^{-7} nM (S/N = 3), the linear regression equation was ΔI (10^{-6} A) =0.5549–0.1858 log (C_{S2}/M), which confirmed the HKUST-CuO could improve sensitivity because of its prominent PEC property. The relative standard deviation (RSD) of the PEC sensor for target DNA detection of 2.0×10^{-4} nM was 7.4%. The proposed DNA biosensor also possessed good specificity and stability. Hence, this reported work was a promising strategy for molecular diagnosis in the bio-analysis field.

Keywords Heterogeneous composite nanoparticles · HKUST-1 · HKUST-CuO · MOF derivative · Photoelectrochemical detection · DNA biosensor

✉ Linjia Huang
huanglinjia@tom.com

✉ Wenhua Gao
whgao@stu.edu.cn

[1] Department of Chemistry and Laboratory for Preparation and Application of Ordered Structural Materials of Guangdong Province, Shantou University, Shantou, Guangdong 515063, People's Republic of China

[2] Department of Natural Sciences, Shantou Polytechnic, Shantou, Guangdong 515078, People's Republic of China

[3] Shantou Food Inspection and Testing Center, Shantou, Guangdong 515041, People's Republic of China

[4] Institute of Chemical Engineering, Guangdong Academy of Sciences, Guangzhou, Guangdong 510665, People's Republic of China

Introduction

Photoelectrochemical (PEC) techniques inherit the advantages of electrochemical methods such as simplicity, portability, and easiness of miniaturization [1–3]. Meanwhile, PEC technique possesses a lower bias potential than that of their electrochemical counterparts, which results potentially in a sensitive sensor [4, 5]. Recently, PEC analysis receives widespread attention in the biochemical field of biomolecules detection such as specific DNA [6], micro-RNA [7, 8], protein kinase [9, 10], and organophosphorus pesticides [11]. Obviously, the property of PEC biosensors is dependent on photoactive materials. The photoactive materials on sensing interface used to be functionalized with the biorecognition substance such as nucleic acids [12], aptamers, and antibodies [13], in which this bio-functionalization effect can inhibit the occurring of redox reaction towards the photoactive materials and

lead to the PEC response magnitude decreasing significantly [14]. Hitherto, most of the conventional photoactive materials such as TiO_2 [15, 16], CdS [17, 18], ZnO [19, 20], Bi_2S_3 [21], MoS_2 [22, 23] and so forth have been employed in constructing the sensing interface of PEC biosensors. However, some inherent defects astrict their real application, for example, the serious photocorrosion, high recombination of photo-produced carriers, poor photostability, and inefficient visible-light harvesting (such as TiO_2 only have the UV-light absorption below 380 nm). Thus, the preparation of innovative photoactive materials with tailorable structure and sensing properties to improving their photoelectric conversion efficiency still has a great many challenges. Also, to boost the sensitivity and accuracy of the analyte test are urgently needed for high-performance PEC sensor.

Metal-organic frameworks (MOFs) also have been considered as a promising electrode-modified material for the application in PEC sensors [24]. However, the poor electrical conductivity of MOFs is still a barrier for PEC assay [25]. To improve this, MOFs as template or precursor are reformed with different methods such as pyrolysis and chemical etching to build a MOF-derived structure with hierarchical pores. These MOF-derived products not only inherit their corresponding morphologies but also connect the virtue of different components such as the metal oxide particles, metal sulfides, C elements, etc., which displayed superior catalytic and electrochemical performances [26–28]. HKUST-1, as the photocatalysis materials merely harvests the UV lights in which it cannot effectively utilize the solar illumination, resulting in a limitation for its practical application [29]. To improve the photocatalytic activities of this type of MOF, coupled HKUST-1 with different bandgap semiconductor materials to form heterogeneous photocatalysts can extend its light utilization from UV to visible region, which also combined novel properties from individual HKUST-1 [30, 31].

Fan et al. [32] synthesized a ZrO_2@HKUST-1 composite by the one-pot reaction that could protect the ZrO_2 nanoparticles from rapid agglomeration and consequently narrowing the bandgap of this composite which enhanced the visible-light photocatalytic effect. Jin et al. [33] reported an HKUST-1 could easily trap the nano-sized CuO nanoparticles in situ, the formed nanocomposites displayed efficient photocatalytic property for hydrogen evolution and methylene blue degradation. However, these commercial ZrO_2 and CuO particles were not homogeneously distributed and may be readily peeled off and fled via the microporous channels of HKUST-1 due to the non-indurative adsorption physically. Therefore, these composites could influence photoactivity enhancement further and decline their stability in practical application. In our work, the CuO component could be obtained by calcining the HKUST-1 precursor and the prepared HKUST-CuO composite with a more harmonious distribution of CuO. Most importantly, the compact HKUST-CuO composite was a benefit for improving the stability of the photocurrent exportation.

Accordingly, the bandgaps of HKUST-1 and HKUST-CuO were estimated to be 2.81 and 1.71 eV, respectively, which could match the wide bandgap (3.2 eV) of TiO_2 to form the heterostructures. PEC results showed that the HKUST-1/TiO_2 and HKUST-CuO/TiO_2 had the enhanced PEC response signals compared to individually HKUST-1 and HKUST-CuO material, which was ascribed to the synergistic effect between the heterogeneous composite. While the PEC response current (2.24 μA) of HKUST-CuO/TiO_2 was about 9.33 times than that of HKUST-1/TiO_2 (0.24 μA) and 74.66 times than that of the mono-component material of TiO_2 (0.03 μA), which could be explained as follows: (1) the hollow and thin-shelled structure of HKUST-CuO could markedly improve visible-light absorption capability; (2) HKUST-CuO presented partly cracked hole was conducive to infiltrate electrolytic solution; (3) the converted CuO component in HKUST-CuO could promote the electron transfer; (4) HKUST-CuO with TiO_2 formed hierarchical bandgap energies architecture further accelerated the photo-generated e^{-1}/h^+ pair separation and migration. The obtained PEC sensing platform of S1/HKUST-CuO/TiO_2/ITO had been successfully applied to measure different colitoxin DNA sequences.

Experimental

Reagents and apparatus

Copper nitrate trihydrate ($Cu(NO_3)_2{\cdot}3H_2O$, 99%), benzene-1,3,5-tricarboxylic acid (BTC, 99%), Chitosan (CS), TiO_2 nanoparticles (40 nm, 99.8%), and phosphate buffer saline (PBS, $Na_2HPO_4{\cdot}12H_2O/KH_2PO_4$) were purchased from Aladdin Chemical Reagent Co., Ltd. (Shanghai, China). Ethanol (98%), NaOH, and acetic acid (36%) were provided by the Guangdong Xilong Chemical Co. Ltd. (Shantou, China). The other reagents were shown in the Electronic Supporting Material (ESM).

The PEC and electrochemical experiments were carried out on a CHI 650E electrochemical analyzer (Shanghai CH Instrument Company). The conventional three-electrode system consisted of bare or modified indium tin oxide (ITO) as working electrode, Ag/AgCl/(3 M KCl) as reference electrode and Pt wire as auxiliary electrode. The irradiation light source was from a 300-W Xe lamp, and the light intensity was measured using a touch screen Thorlabs (PM200, THORLABS, USA). The other details were given in ESM.

Preparation of HKUST-1 and HKUST-CuO composite

The pure HKUST-1 was prepared by the one-step solvothermal method according to the reported literature with a minor modification [34]. In brief, $Cu(NO_3)_2{\cdot}3H_2O$ (0.535 g, 2.21 mmol) and BTC (0.234 g, 1.11 mmol) were separately

added into deionized water (8 mL) and ethanol (8 mL); after stirring at room temperature for 15 min (80 rpm), two solutions were mixed followed with ultrasonication for 10 min under 50 W to obtain the homogeneous solution. Then, the mixture was moved into a 100-mL Teflon-lined stainless steel reactor and heated at 120 °C for 24 h. After natural cooling to room temperature, the blue HKUST-1 particles were carefully collected by centrifugation (8000 rpm, 10 min) and washed with water/ethanol (1:1, volume ratio) several times. Finally, the precipitates were dried at 60 °C for 12 h in a vacuum to obtain the blue HKUST-1 products.

The conversion of HKUST-1 into HKUST-CuO was achieved by calcining the as-fabricated HKUST-1 precursor at 350 °C with the heating rate of 10 °C min^{-1} for 1 h under isolated air. Finally, the black products of HKUST-CuO were obtained.

Fabrication of CS/HKUST-1/TiO_2/ITO and HKUST-CuO/TiO_2/ITO modified electrodes

Prior to modification, the indium tin oxide (ITO) electrodes were ultrasonically washed with acetone, NaOH (1.0 M)/ethanol mixture solution (1:1, volume ratio), and deionized water for each 15 min. After the TiO_2 (8 mg) powder was ultrasonically dispersed in deionized water (4 mL) for 1 h, 8 μL of obtained 2.0 mg mL^{-1} TiO_2 suspension was dropped onto the bare ITO electrode and dried spontaneously. The obtained TiO_2/ITO electrode was calcined at 450 °C under air for 0.5 h to improve the adhesion property of TiO_2 particles on the ITO substrate. Then, 8 μL of 1.5 mg mL^{-1} HKUST-1 blue suspension was cast onto the ITO/TiO_2 electrode surface, after drying at room temperature received the modified electrode of HKUST-1/TiO_2/ITO. 0.3% CS was following prepared by dissolving chitosan powder into 1.0% acetic acid solution for sonicate 15 min, and 5 μL CS solution was introduced onto the above electrode to form a conserved film, the modified electrode named CS/HKUST-1/TiO_2/ITO. The HKUST-CuO/TiO_2/ITO was prepared by annealing the HKUST-1/TiO_2/ITO electrode at 350 °C for 1 h under isolated air.

Probe DNA immobilization and hybridization with different DNA sequences had been reported in ESM

PEC and electrochemical detection

The PEC measurements were carried out in 0.1 M PBS (pH 7.2) using the self-made photoelectric chemical equipment (CHI 650E electrochemical station and a xenon lamp light source) with a three-electrode system, and the light source intensity is 25 mW m^{-2}. The excitation wavelength of 420 nm was switched on every 10 s with 0 V bias voltages. The electrochemical detection had been reported in ESM.

Results and discussion

Characterization of HKUST-1, HKUST-CuO

The morphologies of the prepared HKUST-1and HKUST-CuO were investigated by field-emission SEM. As shown in Fig. 1A, HKUST-1 particles displayed a well-defined octahedral morphology with a sharp edge and smooth surface, demonstrating the prepared samples possessed good crystallinity as well as high purity. From the high-magnification image (inset of Fig. 1A), the edge length and opposite-vertical-apex length of HKUST-1 were about 12 μm and 16 μm, respectively. This result was accordant with the morphological features of HKUST-1 in reported literature [35]. It was noteworthy that HKUST-CuO (Fig. 1B and C) displayed an increased roughness and partly collapsed holes, but the basic octahedral morphology of HKUST-1 was still well maintained. Figure S2A shows the thermogravimetric (TG) analysis of HKUST-1 polyhedral crystal, in which the HKUST-1 precursor could be stable up to approximately 300 °C and a thermal decomposition at the temperature of 350 °C had occurred.

The microstructure of HKUST-CuO was further investigated by high-resolution TEM (HRTEM). As seen in Fig. 1D and E, it could be found that the HKUST-1 and HKUST-CuO particles have the same regular hexagons, confirming that the HKUST-CuO possessed the basic octahedron framework as presented in the SEM discussion. However, compared to purist HKUST-1, the hexagon edge on HKUST-CuO was of more roughness and HKUST-CuO showed a thin crystal with a hollow structure which was caused during the hyperthermia pyrolysis process. The insets of Fig. 1D and E show the selected area electron diffraction (SAED) patterns of HKUST-1 and HKUST-CuO; it could be found that these two samples had the same polycrystalline structure from their concentric diffraction rings. Additionally, it can be seen that the diffraction ring of a single HKUST-1 was not clearer than that of HKUST-CuO, which was plausibly attributed to the thinness and hollow structure of HKUST-CuO crystal but a higher thickness of HKUST-1. The interplanar distance on HKUST-1 and HKUST-CuO were estimated to be 0.28 nm and 0.23 nm (Fig. S1B and C), respectively. The lattice spacing of 0.23 nm corresponds to that of (111) plane of CuO [36], which testified that the HKUST-1 had been converted into HKUST-CuO composite. Figure S1D displayed the EDS elemental mapping of HKUST-CuO, demonstrating that the presence of Cu, C, and O elements in HKUST-CuO.

The powder XRD pattern was performed to survey the crystal structure of HKUST-1 and HKUST-CuO composite. As shown in Fig. 2A, the major peaks indexed on HKUST-1 were well consistent with the face-centered cubic phase of reported literature [35], agreeing with the formation of pure HKUST-1. Compared to the HKUST-1, the absorptive intensity of these above feature peaks on HKUST-CuO declined

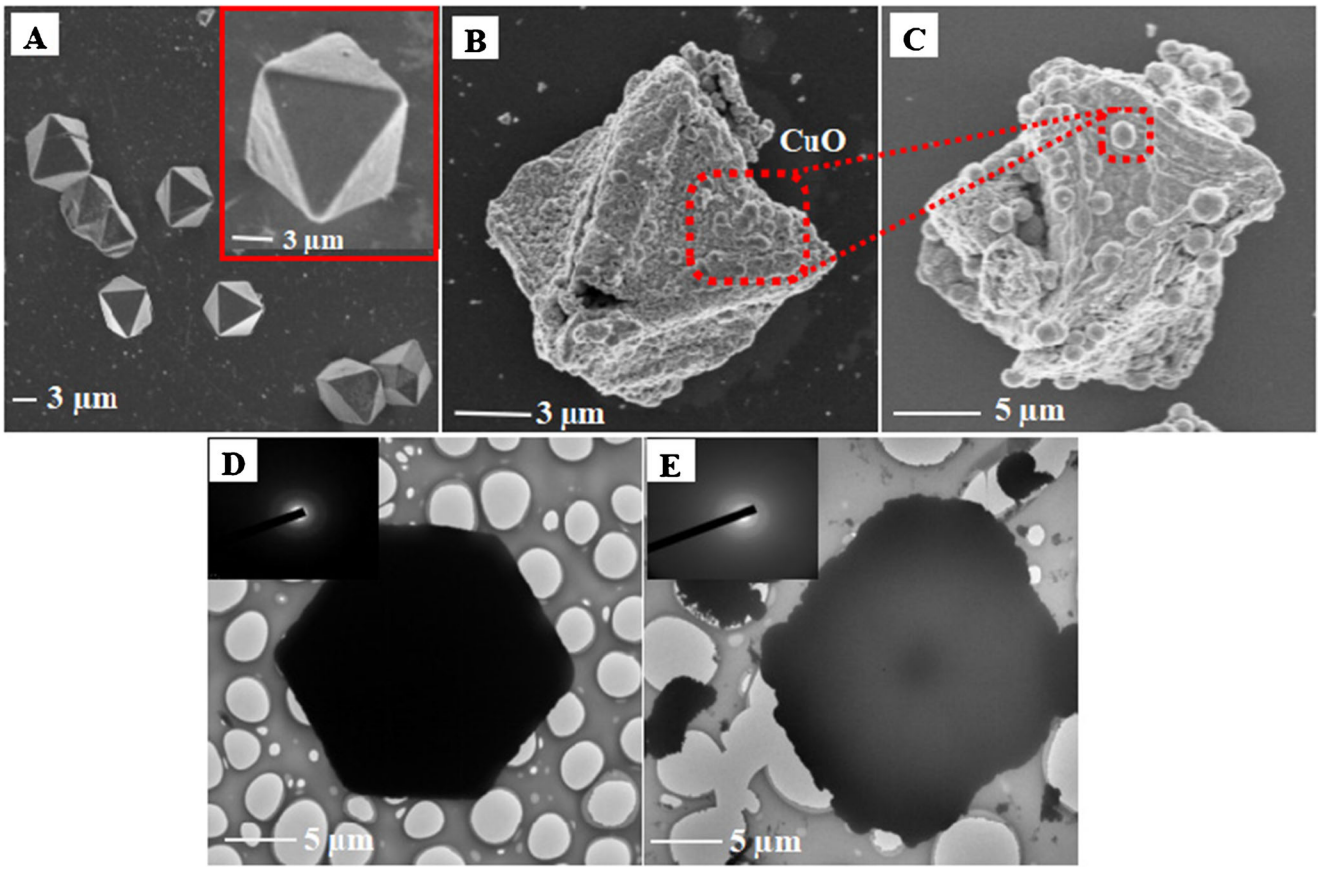

Fig. 1 Low-magnification and high-magnification (inset) SEM images of (A) HKUST-1, (B and C) HKUST-CuO; TEM images of (D) HKUST-1, (E) HKUST-CuO; SAED pattern of (inset of D) HKUST-1 and (inset of E) HKUST-CuO

overtly. The crystallographic planes of (110), (002), (200), (112), (020), and (021) on HKUST-CuO were assigned to the characteristic peaks of CuO (JCPDS No. 44-0706) [37], which confirmed the existence of CuO component in HKUST-CuO. The Raman spectrum and FT-IR spectroscopy of HKUST-1 and HKUST-CuO were also characterized, and the results are illustrated in Fig. S2B and C.

Diffuse reflectance spectroscopy (DRS) was used to investigate the UV-vis absorbance properties of pure TiO_2, HKUST-1/TiO_2, and HKUST-CuO/TiO_2 (Fig. 2B). This proposed absorption spectra showed a common spectral feature combination of TiO_2 in which it absorbed mainly UV light from 220 to 390 nm. However, compared to TiO_2 nanoparticles with a slight photoresponse in the entire visible-light region, HKUST-1/TiO_2, and HKUST-CuO/TiO_2 composites displayed a broad visible-light absorption range from 480 to 800 nm. It was also clearly observed that the highest UV-vis light absorption intensity was obtained on HKUST-CuO/TiO_2 composite. The excellent optical properties may be explained as following two points: (1) HKUST-1 and HKUST-CuO could effectively coordinate the semi-conductive bandgap energy of TiO_2 for increasing the capture of visible light; (2) hollow and thin-shell structure with torn holes on HKUST-CuO was in favor of light incident due to its multiple reflection effect. This result implied that HKUST-1 and its derivative product of HKUST-CuO both had a great potential prospect for the photoactive materials.

X-ray photoelectron spectroscopy (XPS) measurements of HKUST-1 and HKUST-CuO were also carried out. As illustrated in Fig. 2C and Fig. S3C, the prepared materials were both composed of elements of Cu, O, and C. Figure 2D shows that the high-resolution Cu 2p core-level spectra at approximately 933.7 and 953.8 eV correspond to Cu $2p_{3/2}$ and Cu $2p_{1/2}$ peaks, respectively, revealing the copper oxidation state of +2. Meanwhile, two shakeup satellite peaks at 941.3 and 962.1 eV, respectively, which also indicated that the oxidation state of Cu in HKUST-CuO was +2. The O 1s spectrum of HKUST-CuO showed that the peak at 529.6 eV (Fig. S3A) was attributed to the O^{2-} in Cu-O bonding linker. This result corresponds with the XRD survey, indicating the formation of oxidized CuO in HKUST-CuO.

PEC mechanism

The UV-vis DRS of HKUST-1 and HKUST-CuO is displayed in Fig. S2D. It was found that pure HKUST-1 had not owned visible-light property due to its conjugated structure. But on the HKUST-CuO, a continuous and extended light absorption

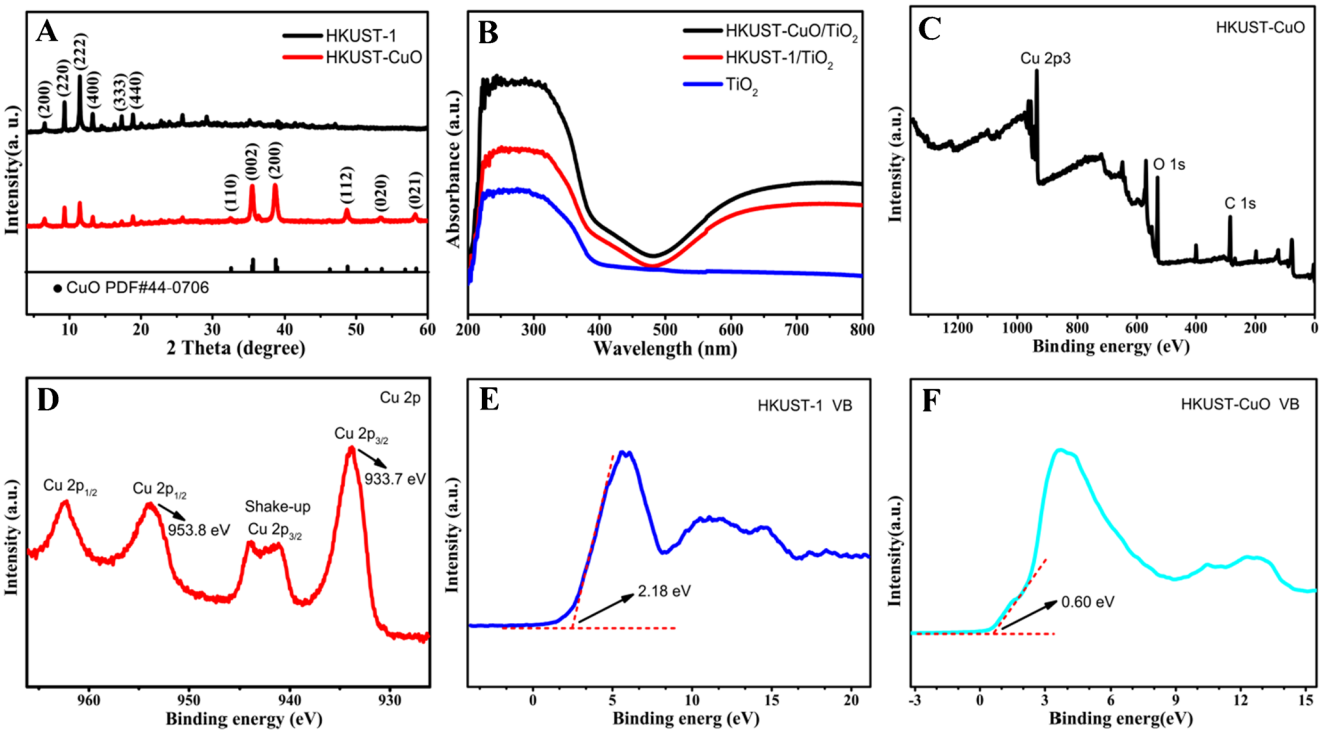

Fig. 2 (A) XRD patterns; (B) UV-vis spectrogram; (C) XPS spectrogram of HKUST-CuO, (D) High-resolution XPS spectrogram of Cu 2p of HKUST-CuO; VB-XPS of (E) HKUST-1 and (F) HKUST-CuO

range from approximately 360 to 800 nm could be seen clearly, suggesting that an enhanced visible-light harvesting ability. The VB potentials of HKUST-1 and HKUST-CuO were monitored by VB-XPS (Fig. 2E and F), and their band edges were 2.18 and 0.60 eV (vs NHE), respectively. Also, the Eg of HKUST-CuO and HKUST-1 can be estimated by using the following equation:

$$ahv = \mathrm{A}\ (hv\text{–Eg})^{1/2}$$

where a, A, and hv are the absorption coefficient, proportionality constant, photon energy, respectively. The Eg values of HKUST-1 and HKUST-CuO were calculated to be approximately 2.81 and 1.71 eV (vs NHE) utilizing the plotted tangents of $(\alpha hv)^2$ versus photon energy (Fig. S2E and F), which demonstrated a reduction Eg value of HKUST-CuO. Besides, based on the empirical formulae of $E_{CB} = E_{VB} - \mathrm{Eg}$, the conduction band (CB) positions of HKUST-1 and HKUST-CuO can be estimated. The E_{CB} and E_{VB} are assigned to the CB and VB edge positions, respectively. Accordingly, the E_{CB} positions of HKUST-1 and HKUST-CuO were estimated to be −0.63 and − 1.11 eV. Additionally, the E_{CB} and E_{VB} positions of TiO_2 were − 0.5 and 2.7 eV (vs NHE) with the Eg value of 3.20 eV (vs NHE) [38].

This result showed that the HKUST-CuO possessed the smallest Eg value as compared with the HKUST-1 and commercial TiO_2, and the CB and VB positions of TiO_2 were lower than both HKUST-CuO and HKUST-1. Hence, the combination of HKUST-1 and HKUST-CuO with TiO_2 had interlaced band structures. When the HKUST-1 and HKUST-CuO were respectively assembled onto TiO_2/ITO electrode, two type heterojunction systems of HKUST-1/TiO_2 and HKUST-CuO/TiO_2 had been formed. Upon photo-excitation, the photo-generated electrons were transferred from the CB of HKUST-1 and HKUST-CuO to the CB of TiO_2, and holes on the VB of TiO_2 were transferred to the VB of HKUST-1 and HKUST-CuO, which led to accelerating the electron-hole pair migration, resulting in enhanced photocurrent responses [39]. The HKUST-CuO/TiO_2 showed a greater photo-generated current effect than HKUST-1/TiO_2, which was attributed to the hollow structure defective of HKUST-CuO as well as the CuO component could extend visible-light utilization range and promote the absorption intensity. Meanwhile, the typical p-type CuO was connected with n-type TiO_2 to form the p-n-type heterojunction, which resulted in an enhanced PEC performance. The photo-generated e^{-1}/h^{+} pair transfer mechanisms of HKUST-1/TiO_2/ITO and HKUST-CuO/TiO_2/ITO electrodes are shown in Scheme 1A.

Electrochemical and PEC behaviors of various modified electrodes

EIS is a valuable tool to reflect the impedance changes of the electrode surfaces, which is used to characterize the process of biosensor construction. From EIS measurements (Fig. 3A), it

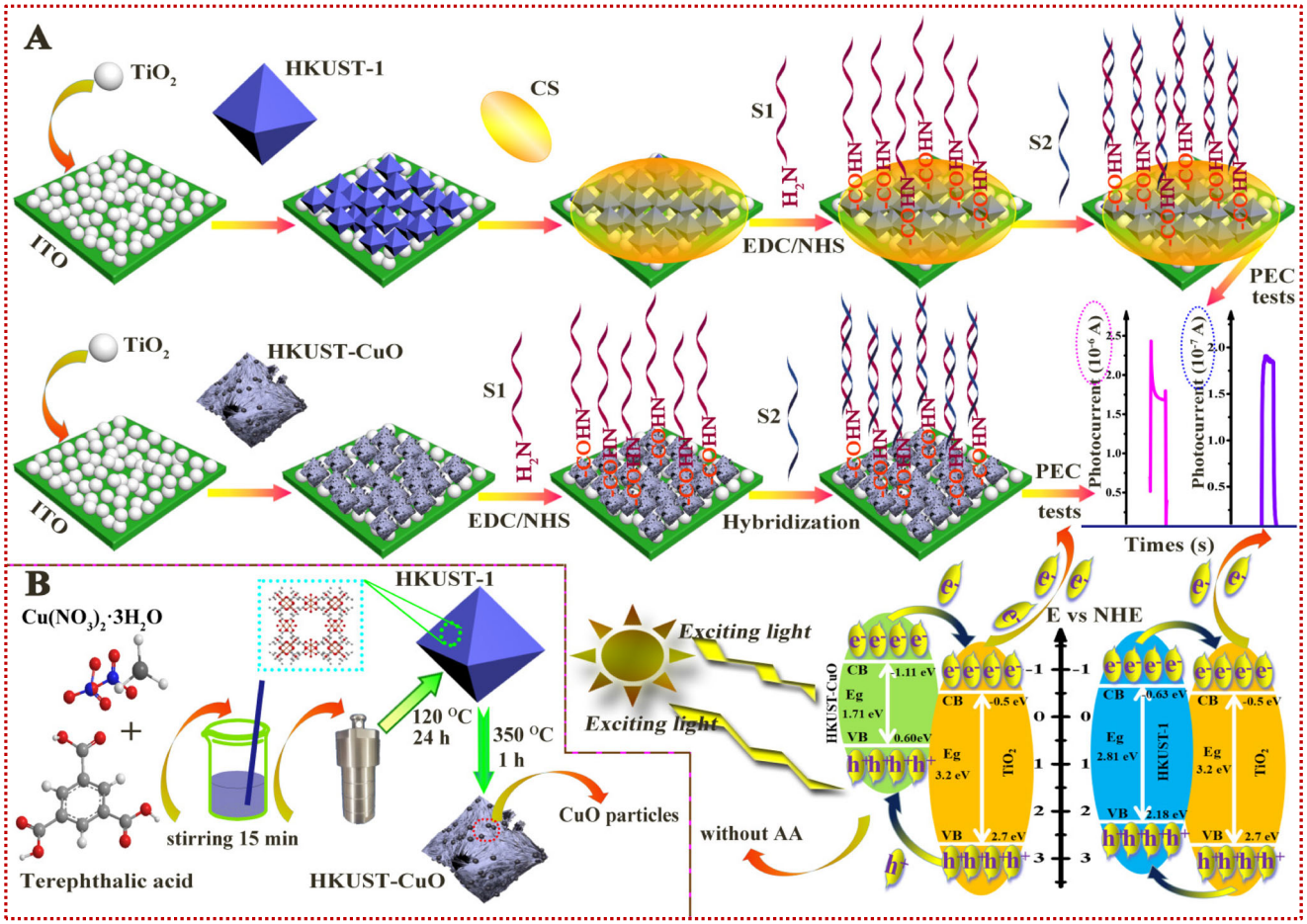

Scheme 1 **A** Schematic illustration of the preparation process of the proposed PEC biosensors for colitoxin DNA detection. **B** The preparation process of HKUST-1 and HKUST-CuO.

could be seen that the small semicircle at the bare ITO electrode corresponds to the R_{et} value of 89.6 Ω (curve a). When the TiO_2 and HKUST-1/TiO_2 were modified onto the bare ITO surface, the R_{et} values were successively increased to 240 Ω and 339 Ω (curves b and c), respectively, which could be ascribed to the poor conductivity of these both substances. On the HKUST-CuO/ITO electrode (curve d), the R_{et} value was estimated to be 125 Ω, indicating that HKUST-CuO could significantly enhance the electronic transport capability due to its thinner layer and hollow structure. On the HKUST-CuO/TiO_2/ITO (curves e) electrode, the R_{et} value increased to 163 Ω, which was ascribed to the thicker film of HKUST-CuO/TiO_2 on the electrode surface may interfere with the electron transfer. After the probe DNA (S1) was anchored on HKUST-CuO/TiO_2/ITO, the R_{et} value again increased to 236 Ω (curve f). This could be explained by the stronger electrostatic repulsion effect between the negatively charged probe DNA and electronegative redox probe of $[Fe(CN)_6]^{3-/4-}$, which also demonstrated that the DNA sensor (S1/HKUST-CuO/TiO_2/ITO) had been successfully fabricated.

To investigate further the construction processes of the DNA biosensors, the photocurrent response signals of different modified electrodes were tested and recorded in 0.1 M PBS (pH 7.2). As shown in Fig. 3B, no photocurrent appeared on the bare ITO (curve a). After bare ITO modified with TiO_2, obtained TiO_2/ITO (curve b) electrode showed a slight photocurrent of about 0.03 μA, indicating that TiO_2 had the poor utilization of visible light. Compared to the TiO_2/ITO, HKUST-CuO/ITO electrode (curve d) displayed an enhancive photocurrent response (0.23 μA), which was attributed to thin-layers and hollow structure of HKUST-CuO could improve visible-spectra absorption performance. When the HKUST-1 was combined with TiO_2 to form the HKUST-1/TiO_2/ITO electrode (curve c), the photocurrent intensity was increased to 0.24 μA. On the HKUST-CuO/TiO_2/ITO electrode (curve e), it was found that a drastically increased photocurrent response of 2.24 μA, which was 9.33-fold than that of HKUST-1/TiO_2/ITO and 9.73-fold than that of HKUST-CuO/ITO electrode, respectively. This result further verified that the HKUST-CuO particles with the CuO component could significantly extend the visible-light range and absorption capacity. Also, the formed heterostructure complex of HKUST-CuO/TiO_2 greatly promoted the separation efficiency of the photo-generated e^{-1}/h^+ pairs on the

electrode interface. When the HKUST-CuO/TiO_2/ITO electrode was modified with S1, the photocurrent signal decreased to 1.92 μA (curve f) due to the low conductivity of the probe DNA, which also confirmed that the probe DNA immobilized sensing platform (S1/HKUST-CuO/TiO_2/ITO) was successfully prepared. Additionally, we had prepared the pure CuO derived from the HKUST-1 precursor and made a comparison on the property of CuO/TiO_2 and HKUST-CuO/TiO_2 composites. These details are shown in Fig. S6.

LSV and OCP measurements of various modified electrodes

Figure 3C shows linear scan voltammograms (LSVs) obtained on TiO_2/ITO, HKUST-1/TiO_2/ITO, and HKUST-CuO/TiO_2/ITO electrodes in 0.1 M Na_2SO_4 under continuous visible-light irradiation. The LSV response indicated that the TiO_2/ITO electrode had scarcely any photo-generated current between the potential range of 0.0 and 1.1 V, which was ascribed to the photo-generated e^{-1}/h^+ pairs with a high recombination rate. When narrow bandgap HKUST-1 was combined with TiO_2 to form the heterojunction complex of HKUST-1/TiO_2, a significant LSV signal was observed. Of note, HKUST-CuO/TiO_2/ITO electrode displayed a greater LSV response than the HKUST-1/TiO_2/ITO or TiO_2/ITO electrode, which was attributed to the CuO component in HKUST-CuO could enhance visible-light harvesting.

Figure 3D shows the OCP response of as-prepared materials with their types at the Fermi level. As seen, in the dark, the modified electrodes of TiO_2/ITO and HKUST-1/TiO_2/ITO both exhibited an upward surface band bending (region I) which were dependent on their potential of redox equilibration [40]. Under illumination, owing to the accumulating photo-generated electrons, OCP on TiO_2/ITO and HKUST-1/TiO_2/ITO electrodes decreased towards a negatively rapid and reached a steady state (region II). When the irradiation was switched off, the OCP gradually increased again (region III), which was ascribed to the recombination of photo-generated charge carriers. However, the OCP behavior of the HKUST-CuO/TiO_2/ITO electrode was opposite compared to TiO_2/ITO electrode. Consequently, the n-type TiO_2 could be presented nominally and mostly to confirm the p-type CuO in HKUST-CuO. Besides, HKUST-CuO/TiO_2/ITO showed a greater OCP response change (ΔOCP) than the TiO_2/ITO or HKUST-1/TiO_2/ITO electrode, demonstrating that the more light-generated electrons and faster charge carriers transition were achieved.

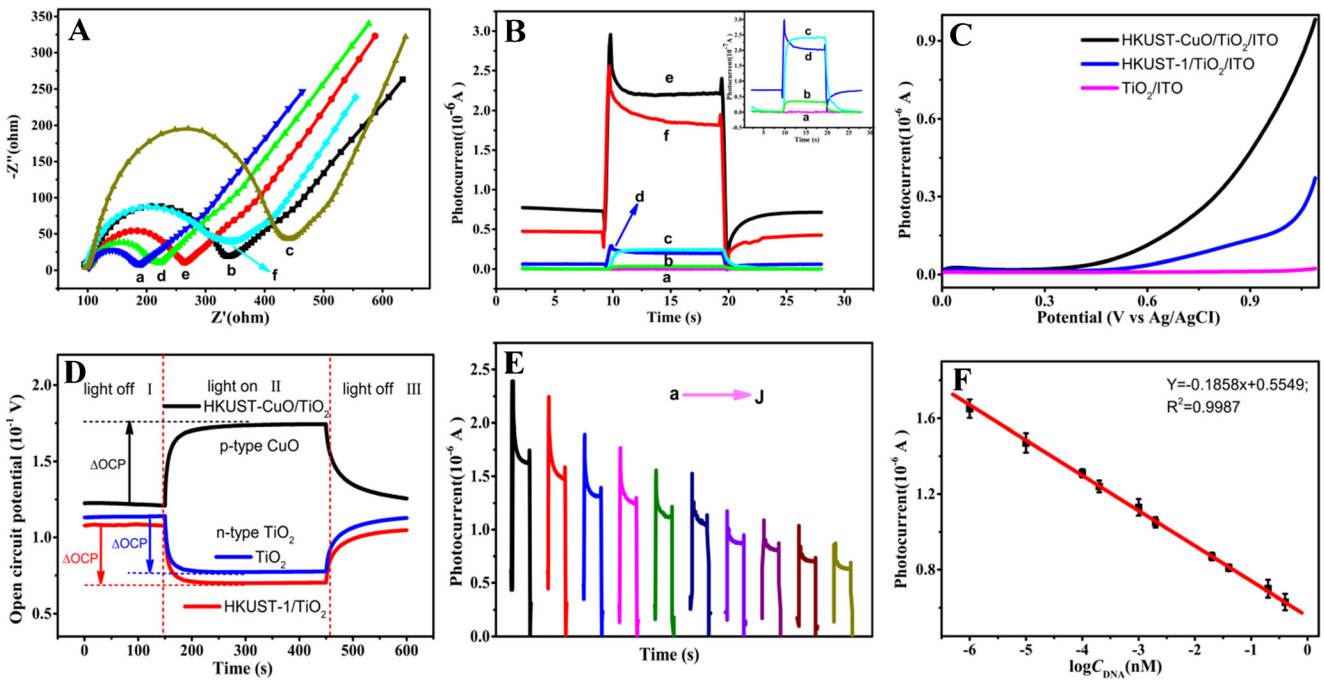

Fig. 3 EIS of (A) bare ITO (a), TiO2/ITO (b), HKUST-1/TiO2/ITO (c), HKUST-CuO/ITO (d), HKUST-CuO/TiO2/ITO (e) and S1/HKUST-CuO/TiO2/ITO (f) in 5 mM K3[Fe(CN)6]/K4[Fe(CN)6] containing 0.1 M KCl; PEC response of (B) bare ITO (a), TiO2/ITO (b), HKUST-1/TiO2/ITO (c), HKUST-CuO/ITO (d), HKUST-CuO/TiO2/ITO (e) and S1/HKUST-CuO/TiO2/ITO (f) in 0.1 M PBS (pH 7.2); **C** LSV pattern in 0.1 M Na2SO4 and (D) OCP curve of the modified electrodes in 0.1 M PBS (pH 7.2); PEC response (E) and the corresponding calibration curve (F) of S1/HKUST-CuO/TiO2/ITO sensor for the detection of different concentrations of target DNA (S2). a-J: 1.0 × 10–6, 1.0 × 10–5, 1.0 × 10–4, 2.0 × 10–4, 1.0 × 10–3, 2.0 × 10–3, 2.0 × 10–2, 4.0 × 10–2, 2.0 × 10–1 and 4.0 × 10–1 nM

Optimization of experimental conditions had been reported in ESM

Performance of the biosensors for colitoxin DNA detection

Figure 3E shows that the photocurrent signals decreased gradually after the S1/HKUST-CuO/TiO_2/ITO biosensor hybridization with the increasing target DNA concentration (C_{S2}) under the optimal experimental conditions. The photocurrent change values (ΔI) were commendably proportional to the logarithm of the target DNA concentration (log C_{S2}). The linear detection range of S2 was from 1.0×10^{-6} nM to 4.0×10^{-1} nM with a low detection limit of about 3.37×10^{-7} nM based on a signal-to-noise ratio of 3, the linear regression equation was ΔI (10^{-6} A) =0.5549–0.1858 log (C_{S2}/M) with the R^2 value of 0.9987 (Fig. 3F). Obtained results exhibited higher sensitivity than S1/CS/HKUST-1/TiO_2/ITO biosensor (Fig. S4) and other DNA sensing platforms (Table S1) through comparison with their linear detection ranges and detection limit values. The superior analysis property of S1/HKUST-CuO/TiO_2/ITO could be ascribed to the heterogeneous HKUST-CuO/TiO_2 composite with the positively CuO component.

Selectivity, stability, and precision of the PEC biosensors

The stability of the proposed PEC biosensor was also examined. As seen in Fig. 4A, with the PEC response of S1/HKUST-CuO/TiO_2/ITO electrode hybridization with target DNA of 5.0×10^{-6} nM under irradiation cycles for 400 s and ten on/off, it was found that no significant photocurrent change, demonstrating the developed PEC biosensor had steady photocurrent response towards the target DNA (S2). Meanwhile, the stability of the S2-S1/HKUST-1/TiO_2/ITO hybridization electrode is investigated in Fig. S4D. Besides, the S1/HKUST-CuO/TiO_2/ITO was stored at 4 °C for a week, and the photocurrent decreased to 94.1%; when the

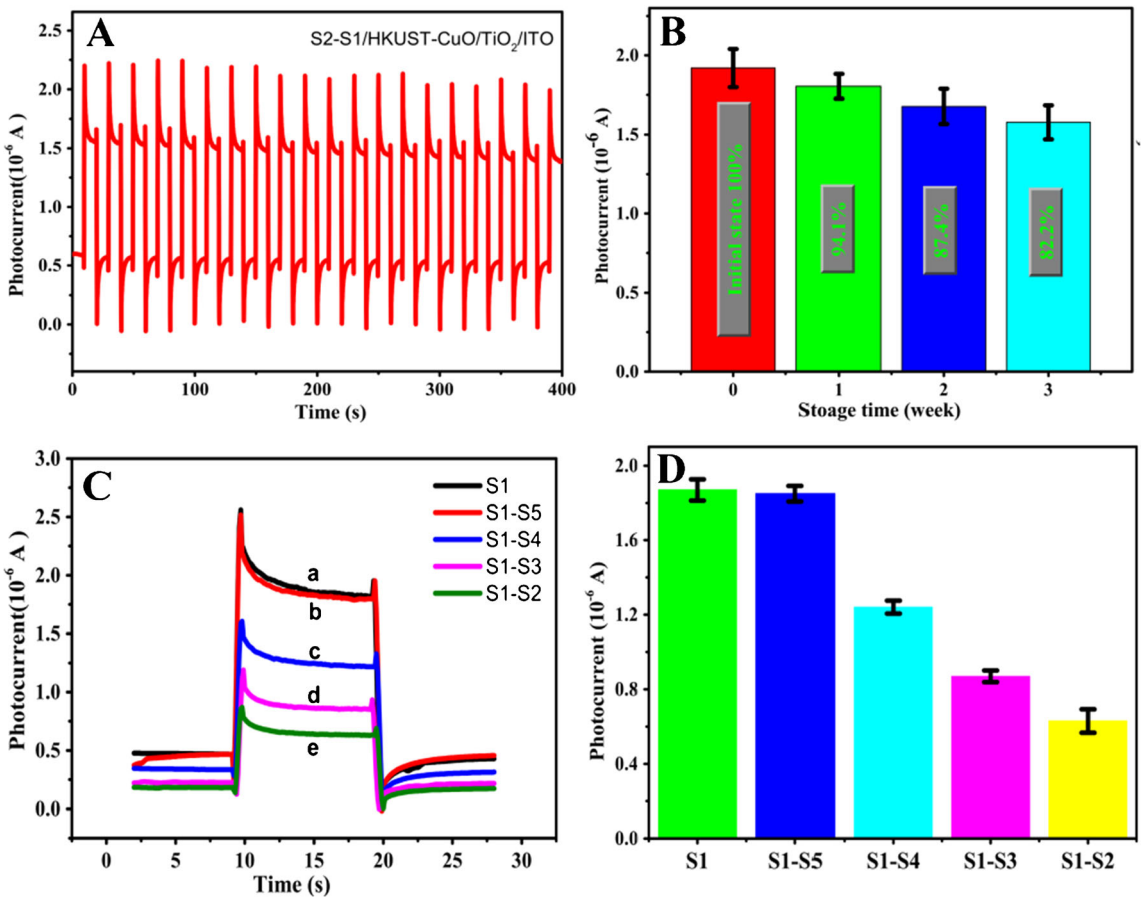

Fig. 4 Time-based photocurrent response of (A) S2-S1/HKUST-CuO/TiO2/ITO electrode in 0.1 M PBS (pH 7.2) with the light on and off cycles; the photocurrent responses of (B) as-prepared biosensor after different storage time (week) in PBS (0.1 M, pH 7.2); selectivity of (C) S1/HKUST-CuO/TiO2/ITO (a) hybridization with 1.0 nM different target DNA mixtures: non-complementary DNA (S5) (b), three-base mismatch DNA (S4) (c), single-base mismatch DNA (S3) (d) and complementary DNA (S2) (e); the corresponding histogram of photocurrent values on the biosensor of (D) S1/HKUST-CuO/TiO2/ITO hybridization with special DNA sequences

storage time was at 2 weeks, the photocurrent reduced to 87.4% (Fig. 4B), suggesting that the modified electrode also had the receivable stability.

The selectivity of fabricated DNA sensors was investigated by hybridization with special DNA sequences (S2, S5, S3, and S4). Figure 4C shows that S1/HKUST-CuO/TiO_2/ITO (curve a) had the highest PEC response signal. However, after hybridization with S2 (curve e), the PEC signals significantly decreased, indicating the efficient hybridization reaction occurrence on the electrode surface. When the biosensor was hybridized with S5 (curve b), there was a negligible change of the photocurrent response, suggesting that the non-specific absorption did not occur. When biosensor was hybridized with S3, S4 (curve d, c), the decreased photocurrent was still higher than that obtained on the hybridized electrode with S2 (the corresponding histogram of photocurrent values shown in Fig. 4D), which implied the S3 and S4 DNA sequences only occurred at partial hybridization with S1. The selectivity experiment demonstrated that the developed biosensor possessed good selectivity.

Precision is also a critical factor in developing high property biosensors. The precision of the PEC DNA sensors was investigated by comparing the photocurrents of three equilibrium results of S1/HKUST-CuO/TiO_2/ITO electrode after hybridization with 2.0×10^{-4} nM target DNA; the obtained relative standard deviation (RSD) was corresponding to 7.4%, which indicated that the fabricated PEC biosensor owned acceptable precision.

Conclusion

The prepared photoactive materials of HKUST-1/TiO_2 and HKUST-CuO/TiO_2 both had heterojunction architectures which could promote the photocurrent response signals. But the HKUST-CuO displayed a great improvement capability for the visible-light harvesting than its precursor of HKUST-1, which was attributed to the hollow and thin-shell structure of HKUST-CuO with the CuO component. Besides, compared with the HKUST-1/TiO_2 heterojunction, HKUST-CuO/TiO_2 exhibited a stronger PEC response due to the formed p-n-type composite. Benefiting from the outstanding photoactive performance of HKUST-CuO/TiO_2, the probe DNA (S1) immobilized electrode of S1/HKUST-CuO/TiO_2/ITO was prepared successfully and applied for the hybridization with target DNA (S2). This sensing platform exhibited a better sensitivity than the S1/CS/HKUST-1/TiO_2/ITO sensor through a comparison with their detection linear ranges and detection limit values. This work deeply explored the PEC properties of the Cu-MOFs derivative of HKUST-CuO, and the application of HKUST-CuO/TiO_2 composite as the photoactive material in PEC sensor was initially studied. Further work will be carried out on the construction of other novel heterojunctions and the application of other fields.

Supplementary Information The online version contains supplementary material available at https://doi.org/10.1007/s00604-021-04999-4.

Acknowledgements We are grateful for the financial support from Guangdong Basic and Applied Basic Research Foundation (No. 2019A1515010618), the Guangdong Special Funds for the Science & Technology Project (No. 2019ST029 and No. 2019ST089), 2020 Li Ka Shing Foundation Cross-Disciplinary Research Grant (Project Number 2020LKSFG06C), and Shantou Polytechnic Supported Project (No. 2019SZK2019Y01).

Declarations

Conflict of interest The authors declare no competing interests.

References

1. Zhang N, Ruan Y, Zhang L, Zhao W, Xu J, Chen H (2018) Nanochannels photoelectrochemical biosensor. Anal Chem 90: 2341–2347
2. Zhang H, Zhao L, Geng F, Guo L-H, Wan B, Yang Y (2016) Carbon dots decorated graphitic carbon nitride as an efficient metal-free photocatalyst for phenol degradation. Appl Catal B Environ 180:656–662
3. Wang J, Song M, Hu C, Wu K (2018) Portable, self-powered, and light-addressable photoelectrochemical sensing platforms using pH meter readouts for high-throughput screening of thrombin inhibitor drugs. Anal Chem 90:9366–9373
4. Singh AP, Kodan N, Mehta BR, Held A, Mayrhofer L, Moseler M (2016) Band edge engineering in $BiVO_4$/TiO_2 heterostructure: enhanced photoelectrochemical performance through improved charge transfer. ACS Catal 6:5311–5318
5. Cheng W, Pan J, Yang J, Zheng Z, Lu F, Chen Y, Gao W (2018) A photoelectrochemical aptasensor for thrombin based on the use of carbon quantum dot-sensitized TiO_2 and visible-light photoelectrochemical activity. Microchim Acta 185:263
6. Sui C, Zhou Y, Wang M, Yin H, Wang P, Ai S (2018) Aptamer-based photoelectrochemical biosensor for antibiotic detection using ferrocene modified DNA as both aptamer and electron donor. Sensors Actuators B Chem 266:514–521
7. Zhu M, Mu X, Deng H, Zhong X, Yuan R, Yuan Y (2019) Ultrasensitive photoelectrochemical biosensor for MiRNA-21 assay based on target-catalyzed hairpin assembly coupled with distance-controllable multiple signal amplification. Chem Commun 55:9622–9625
8. Hou T, Xu N, Wang W, Ge L, Li F (2018) Truly immobilization-free diffusivity-mediated photoelectrochemical biosensing strategy for facile and highly sensitive microRNA assay. Anal Chem 90: 9591–9597
9. Shu J, Qiu Z, Lv S, Zhang K, Tang D (2018) Plasmonic enhancement coupling with defect-engineered TiO_2-x: a mode for sensitive photoelectrochemical biosensing. Anal Chem 90:2425–2429
10. Chen Y, Zhou Y, Wu H, Wang L, Guo R, Yin H, Wang J, Ai S (2020) Photoelectrochemical assay for histone acetyltransferase based on polydopamine sensitized layered WS_2. Sensors Actuators B Chem 319:128261
11. Cheng W, Zheng Z, Yang J, Chen M, Yao Q, Chen Y, Gao W (2019) The visible light-driven and self-powered

photoelectrochemical biosensor for organophosphate pesticides detection based on nitrogen doped carbon quantum dots for the signal amplification. Electrochim Acta 296:627–636
12. Lv S, Zhang K, Zeng Y, Tang D (2018) Double photosystems based 'z-scheme' photoelectrochemical sensing mode for ultrasensitive detection of disease biomarker accompanying three dimensional DNA walker. Anal Chem 90:7086–7093
13. Zang Y, Lei J, Ju H (2017) Principles and applications of photoelectrochemical sensing strategies based on biofunctionalized nanostructures. Biosens Bioelectron 96:8–16
14. Saha S, Chan Y, Soleymani L (2018) Enhancing the photoelectrochemical response of DNA biosensors using wrinkled interfaces. ACS Appl Mater Interfaces 10:31178–31185
15. Wu F, Yu Y, Yang H, German LN, Li Z, Chen J, Yang W, Huang L, Shi W, Wang L, Wang X (2017) Simultaneous enhancement of charge separation and hole transportation in a TiO_2–$SrTiO_3$ core–shell nanowire photoelectrochemical system. Adv Mater 29: 1701432
16. Chen Y, Yin H, Li F, Zhou J, Wang L, Wang J, Ai S (2020) Polydopamine-sensitized WS_2/black-TiO_2 heterojunction for histone acetyltransferase detection with enhanced visible-light-driven photoelectrochemical activity. Chem Eng J 393:124707
17. Hou T, Zhang L, Sun X, Li F (2016) Biphasic photoelectrochemical sensing strategy based on in situ formation of CdS quantum dots for highly sensitive detection of acetylcholinesterase activity and inhibition. Biosens Bioelectron 75:359–364
18. Tang J, Li J, Xiong P, Sun Y, Zeng Z, Tian X, Tang D (2020) Rolling circle amplification promoted magneto-controlled photoelectrochemical biosensor for organophosphorus pesticides based on dissolution of core-shell MnO_2 nanoflower@CdS mediated by butyrylcholinesterase. Microchim Acta 187:450
19. Kargar A, Sun K, Jing Y, Choi C, Jeong H, Zhou Y, Madsen K, Naughton P, Jin S, Jung GY, Wang D (2013) Tailoring n-ZnO/p-Si branched nanowire heterostructures for selective photoelectrochemical water oxidation or reduction. Nano Lett 13: 3017–3022
20. Zhan WW, Kuang Q, Zhou JZ, Kong XJ, Xie ZX, Zheng LS (2013) Semiconductor@metal–organic framework core–shell heterostructures: a case of ZnO@ZIF-8 nanorods with selective photoelectrochemical response. J Am Chem Soc 135:1926–1933
21. Gao X, Wu HB, Zheng L, Zhong Y, Hu Y, Lou XWD (2014) Formation of mesoporous heterostructured $BiVO_4$/Bi_2S_3 hollow discoids with enhanced photoactivity. Angew Chem Int Ed 126: 6027–6031
22. Wang Y, Chen F, Ye X, Wu T, Wu K, Li C (2017) Photoelectrochemical immunosensing of tetrabromobisphenol A based on the enhanced effect of dodecahedral gold nanocrystals/MoS_2 nanosheets. Sensors Actuators B Chem 245:205–212
23. Pesci FM, Sokolikova MS, Grotta C, Sherrell PC, Reale F, Sharda K, Ni N, Palczynski P, Mattevi C (2017) MoS_2/WS_2 heterojunction for photoelectrochemical water oxidation. ACS Catal 7:4990–4998
24. Zhang X, Peng J, Ding Y, Zheng D, Lin Y, Chen Y, Gao W (2020) Rationally designed hierarchical hollow ZnCdS@MoS_2 heterostructured cages with efficient separation of photogenerated carriers for photoelectrochemical aptasensing of lincomycin. Sensors Actuators B Chem 306:127552
25. Xu C, Liu L, Wu C, Wu K (2020) Unique 3D heterostructures assembled by quasi-2D Ni-MOF and CNTs for ultrasensitive electrochemical sensing of bisphenol A. Sensors Actuators B Chem 310:127885
26. Wang Q, Gao F, Xu B, Cai F, Zhan F, Gao F, Wang Q (2017) ZIF-67 derived amorphous $CoNi_2S_4$ nanocages with nanosheet arrays on the shell for a high-performance asymmetric supercapacitor. Chem Eng J 327:387–396
27. Tang R, Zhou S, Yuan Z, Yin L (2017) Metal-organic framework derived Co_3O_4/TiO_2/Si heterostructured nanorod array photoanodes for efficient photoelectrochemical water oxidation. Adv Funct Mater 27:1701102
28. Cao Y, Wang L, Wang C, Su D, Liu Y, Hu X (2019) Photoelectrochemical determination of malathion by using CuO modified with a metal-organic framework of type Cu-BTC. Microchim Acta 186:481
29. Qiu JH, Zhang XG, Feng Y, Zhang XF, Wang HT, Yao JF (2018) Modified metalorganic frameworks as photocatalysts. Appl Catal B Environ 231:317–342
30. Low JX, Yu JG, Jaroniec M, Wageh S, Al-Ghamdi AA (2017) Heterojunction photocatalysts. Adv Mater 29:1601694
31. Li XY, Pi YH, Hou QQ, Yu H, Li Z, Li YW et al (2018) Amorphous TiO_2@NH_2-MIL-125(Ti) homologous MOF-encapsulated heterostructures with enhanced photocatalytic activity. Chem Commun 54:1917–1920
32. Fan C, Dong H, Liang Y, Yang J, Tang G, Zhang W, Cao Y (2019) Sustainable synthesis of HKUST-1 and its composite by biocompatible ionic liquid for enhancing visible-light photocatalytic performance. J Clean Prod 208:353–362
33. Jin M, Qian X, Gao J, Chen J, Hensley DK, Ho HC, Percoco RJ, Ritzi CM, Yue Y (2019) Solvent-free synthesis of CuO/HKUST-1 composite and its photocatalytic application. Inorg Chem 58:8332–8338
34. Wang Q, Yang Y, Gao F, Ni J, Zhang Y, Lin Z (2016) Graphene oxide directed one-step synthesis of flowerlike graphene@HKUST-1 for enzyme-free detection of hydrogen peroxide in biological samples. ACS Appl Mater Interfaces 8:32477–32487
35. Yang Y, Wang Q, Qiu W, Guo H, Gao F (2016) Covalent immobilization of $Cu_3(btc)_2$ at chitosan-electroreduced graphene oxide hybrid film and its application for simultaneous detection of dihydroxybenzene isomers. J Phys Chem C 120:9794–9803
36. Wang Y, Lü Y, Zhan W, Xie Z, Kuang Q, Lansun Z (2015) Synthesis of porous Cu_2O/CuO cages using Cu-based metal-organic-framework as templates and their gas-sensing properties. J Mater Chem A 3:12796–12803
37. Hu XS, Li C, Lou XB, Yang Q, Hu BW (2017) Hierarchical CuO octahedra inherited from copper metal-organic frameworks: high-rate and high-capacity lithium-ion storage materials stimulated by pseudocapacitance. J Mater Chem A 5:12828–12837
38. Li K, Chai B, Peng T, Mao J, Zan L (2013) Preparation of agIn5S8/TiO_2 heterojunction nanocomposite and its enhanced photocatalytic H_2 production property under visible light. ACS Catal 3:170–177
39. Li H, Zhou Y, Tu W, Ye J, Zou Z (2015) State-of-the-art progress in diverse heterostructured photocatalysts toward promoting photocatalytic performance. Adv Funct Mater 25:998–1013
40. Kamimura J, Bogdanoff P, Ramsteiner M, Corfdir P, Feix F, Geelhaar L, Riechert H (2017) P-type doping of GaN nanowires characterized by photoelectrochemical measurements. Nano Lett 17:1529–1537